J. Biophotonics **7**, No. 3–4, 180–188 (2014) / **DOI** 10.1002/jbio.201300167

Journal of BIOPHOTONICS

FULL ARTICLE

Assessing the challenges of Fourier transform infrared spectroscopic analysis of blood serum

Caryn Hughes[1,2], *Michael Brown*[2], *Graeme Clemens*[1,3], *Alex Henderson*[1,3], *Geraldine Monjardez*[1,3], *Noel W. Clarke*[2,4], *and Peter Gardner*[*,1,3]

[1] Manchester Institute of Biotechnology, The University of Manchester, 131 Princess Street, Manchester, M1 7DN, UK
[2] Genito Urinary Cancer Research Group, Institute of Cancer Sciences, Paterson Building, The University of Manchester, Manchester Academic Health Science Centre, The Christie NHS Foundation Trust, Manchester, M20 4BX, UK
[3] School of Chemical Engineering and Analytical Science, The University of Manchester, Oxford Road, Manchester, M13 9PL, UK
[4] Department of Urology, The Christie NHS Foundation Trust, Manchester, UK, M20 4BX, UK

Received 17 October 2013, revised 30 December 2013, accepted 13 January 2014
Published online 31 January 2014

Key words: FTIR, ATR, transmission, blood, serum, prostate cancer

There are many approaches to measuring the infrared spectrum of a blood serum sample. Naturally, each approach will have both advantages and disadvantages. We report on the progress of the application of infrared spectroscopy in the field of blood serum analysis towards clinical application, with a focus on prostate cancer. In order to perform a high-powered study with clinical relevance, choosing the most suitable approach must undergo careful consideration. We review the possibilities of using different sample preparation methods and speculate upon the potential pitfalls of both transmission and attenuated total reflectance (ATR) techniques.

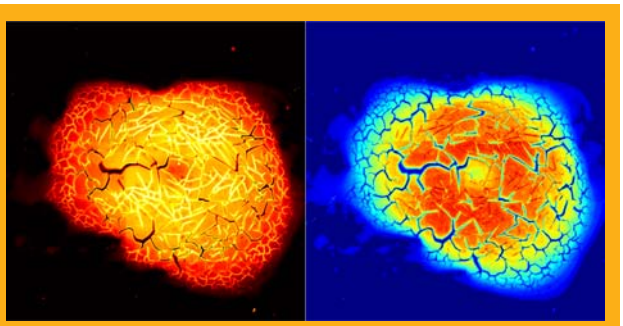

Total intensity of absorbance heat map (**l**) and integrated protein absorbance area map (**r**) of a dried human blood serum sample displaying chemical heterogeneity.

1. Introduction

Infrared spectroscopic study of blood-based samples is not a new concept [1–3]. Over the years, there have been frequent reports of both transmission and attenuated total reflectance (ATR) measurements of blood-derived samples for diagnostic applications such as bovine spongiform encephalopathy (BSE) [4], cardiology [5], bladder cancer [6], brain cancer [7] and ovarian cancer [8]. On first inspection, the application of infrared spectroscopy for the analysis of blood serum may seem straight forward to the uninitiated. There are, in fact, multiple approach combinations one can take to perform such analysis and options must be carefully considered. In order to proceed with the most suitable method often the

* Corresponding author: e-mail: peter.gardner@manchester.ac.uk

configuration must be tailored for the specific sample. For instance, should the sample be kept hydrated, allowed to dry naturally or dried with assistance? What determines the criteria for a sample to be classified as dried? This is not so easy given the complex physical properties of blood serum. Should the technique be high-throughput? Clearly, speed of data acquisition is important when a diagnostic test is established. If embarking upon spectral biomarker discovery for a new diagnostic target, however, this is less of an issue and reliability of the data will preside over speed.

The focus of our blood research is prostate cancer (CaP), therefore we demonstrate the use of different methods on a sample of male human blood serum as a model. In current investigations of methodology, sub-fractioning of serum samples is yet another configuration option to consider [5, 7]. Inevitably this approach adds to the sample preparation, however, at this early stage of analysis, separating the whole serum into sub-fractions also reduces the spectral complexity (Figure 1). When investigating the potential of a new diagnostic test for CaP, there are further advantages; the molecular forms of serum prostate specific antigen (PSA) span the 30–90 kDa range [9]. The PSA test is notorious for delivering false positive results in CaP diagnosis [10, 11]

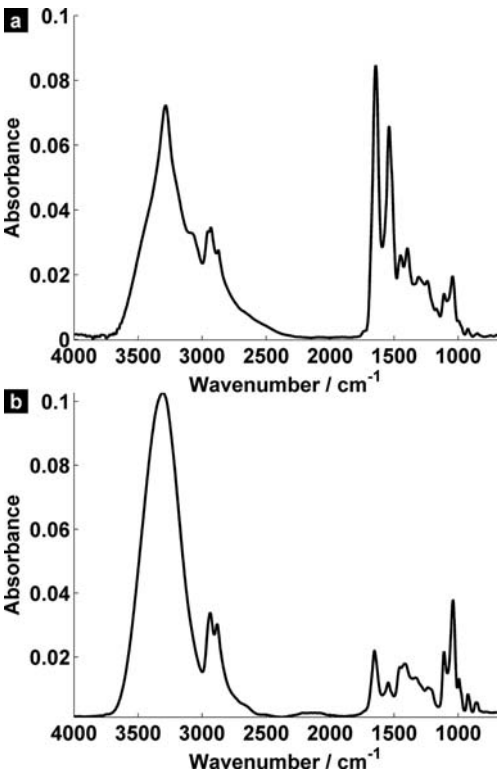

Figure 1 Example ATR spectra of (**a**) >100 kDa and (**b**) 10–100 kDa filtered serum, acquired 30 minutes after direct application.

and hence there is an urgent need for reliable CaP biomarkers [12].

Recently there have been advances in proteomic biomarker discovery [12, 13] indicating various markers for diagnostic potential including those with a molecular weight >100 kDa [14]. Another advantage of analysing the >100 kDa fraction is to avoid the highly abundant human serum albumin (67 kDa [15]), a molecule that could otherwise mask spectral discrimination of disease state. We are of course keen to investigate other fractions, such as the 10–100 kDa molecular range.

By fraction analysis we increase the sensitivity of detection for lower abundance molecules in this mass range that may be otherwise lost due to underlying absorbance peaks from higher mass proteins (Figure 1b). The biochemical composition of the 10–100 kDa fraction is clearly very different from the >100 kDa fraction and may present its own unique challenges for analysis; Whilst the higher molecular weight fraction displays a general biological absorbance spectrum with familiar ratios of protein, lipid and carbohydrate contributions, the lower molecular weight fraction spectrum displays a different signature. For instance, there are only two C−H stretching bands present in the lipid region at 2934 cm^{-1} and 2880 cm^{-1}. No distinctive methyl or methylene peaks infers that a lack of lipid structure is present within the sample. The sample is also rich in carbohydrate chemistry and the spectral profile is similar to that of glycerol [16, 17]. In addition to this profile, however, the 10–100 kDa fraction spectrum contains amide I and II protein peaks, suggestive of a high concentration of blood-related glycoproteins. Despite the fact that simple sugar molecules are too small to be retained in the 10–100 kDa fraction, the use of this fraction for clinical diagnosis may also not be advisable; the potential sensitivity to blood sugar spikes from factors such as diet or hormone treatment could influence the levels of certain glycoproteins within the blood.

While the comparison of techniques has been considered previously [18], we also highlight potential advantages, pitfalls and the need for sample-specific tailoring with the use of serum fractioning. In particular, we outline transmission measurement obstacles with the novel use of infrared hyperspectral imaging and demonstrate how imaging may be used in combination with previously considered configurations by cluster analysis.

The choice of measurement technique is particularly relevant in the light of the recent controversy regarding the use of low-e substrates for either transflection measurements or as a support for top down micro-ATR. In transflection-mode, the spectra are modulated by the electric field standing wave effect and therefore, unless the thickness of the biological film can be controlled to sub-micron levels, the re-

sults are likely to be unreliable [19–21]. In the case of top down micro-ATR on low-e slides, there is a real risk of substrate contributions breaking through into the sample spectrum if the sample film is too thin [22].

In this paper, we restrict our discussion to transmission measurements of dried blood serum on calcium fluoride and in the case of ATR serum, films directly deposited on the ATR crystal. We have not considered the use of a fluidic system for hydration studies as we are using processed blood serum; the technique is more suited to continuous monitoring for whole blood of patients, as previously assessed [23].

2. Experimental

2.1 Sample preparation

Patient samples used in this project were collected from consenting men with ethical approval (Trent MREC 01/4/061 & Salford and Trafford LREC Number 02/ST/122). Each sample was removed from cryogenic storage and left to thaw on ice. Stock serum (50 µl) was added to d.d.H_2O (450 µL) to achieve a 1 : 10 dilution.

The serum was filtered and separated in three different molecular weight fractions (>100 kDa, 10–100 kDa and <10 kDa). For the filtration process, the diluted serum (500 µL) was dispensed into an Amicon® Ultra-0.5 Centrifugal filter 100 k column, which was inserted into a collection tube (Figure 2i). The tube was placed inside a micro-centrifuge and spun at RT for 15 minutes at 14,000 × g. This resulted in filtrate, containing molecules that were smaller than 100 kDa, at the bottom of the collection tube (Figure 2ii).

The fraction containing molecules >100 kDa was retained in the filter column which was immediately turned upside-down and placed inside a new collection tube (Figure 2iii). This fraction was spun for 2 minutes at 1,000 × g to collect the concentrate (~15 µL (15/500)), which was subsequently stored on ice for further sample preparation (Figure 2iv). The remaining filtrate (~485 µL) was then placed into an Amicon® Ultra-0.5 Centrifugal filter 10 k column, inserted into a new collection tube and spun using the micro-centrifuge for 15 minutes at 14,000 × g. The filtrate contained the fraction of molecules smaller than 10 kDa (~455 µL). The 10 kDa fraction was considered too dilute and not used in this particular study. The concentrate remaining was the 10–100 kDa fraction. This was again turned upside-down into a new collection tube and spun for 2 minutes at 1,000 × g to collect the concentrate (~30 µL (30/485)).

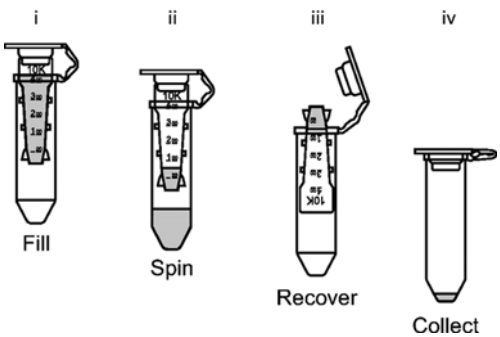

Figure 2 Amicon® Ultra-0.5 centrifugal filter column protocol

For infrared data acquisition, 1 uL of sample was then placed either on a calcium fluoride substrate or directly onto an ATR germanium crystal. For transmission experiments, the samples were left to dry at ambient temperature for 24 hours. For the ATR measurements, a spectrum was recorded initially after the sample was applied to the crystal and then every 3 minutes for a period of one hour.

2.2 Data acquisition methods

All infrared data was captured using a Varian 670-IR spectrometer coupled with a Varian 620-IR imaging microscope (Agilent Technologies, CA) with either a 128 × 128 pixel liquid nitrogen-cooled Mercury-Cadmium-Telluride (MCT) focal plane array or single point MCT detector. The sampling aperture of the single point detector was 550 µm × 550 µm. All spectra were collected at a spectral resolution of 4 cm^{-1}, with the co-addition of 32 scans for sample spectra and 128 scans for the background spectra. Due to a combination of detector and CaF_2 substrate limits, spectra were collected at 800–4000 cm^{-1} and 900–4000 cm^{-1} for single-point and FPA transmission mode respectively. For ATR, data was collected between 700–4000 cm^{-1} since the sample was adsorbed directly to the crystal and the range only limited by the MCT single-point detector.

2.3 Data analysis

Apart from Figure 1 where spectral ratios have been compensated using an ATR correction (Varian Resolutions Pro 4.0), single-point spectra are presented in their raw format to clearly illustrate any potential issues.

The imaging analysis was pre-processed as previously described [24]. The processing was performed in order to demonstrate whether localised

regions of similar molecular chemistry could be identified after removing sample thickness as an immediate factor (as explained in the results and discussion, this is not completely possible if saturation occurs). Briefly, imaging data underwent quality control to remove non-sample related pixel spectra by using an amide I peak area threshold. Secondly, the data range was cut to remove the CO_2 spectral region and subsequently transformed to the first derivative with Savitzky-Golay filtering and 13 smoothing points. To reduce the dimensionality of the data, principal component analysis (PCA) was performed and *k*-means clustering applied to the first 10 principal components for the >100 kDa and 10–100 kDa image respectively.

3. Results and discussion

3.1 Transmission measurements

A total of 25 single point transmission-mode spectra were collected from a dried >100 kDa serum sample in random locations (Figure 3a). It can be observed that there are clearly thickness differences in the dried serum spot.

The thickness of the sample has not caused obvious saturation, yet the danger of the spectral acquisition of such a sample in transmission mode is immediately evident. On the basis of the different band structures observed in the amide I and II regions (Figure 3b), one could be led to conclude that the protein structure is completely different in the thicker regions of the sample where the absorbance is relatively high. This is partly true, due to the well-known 'coffee-ring' chromatography effect [25], molecules of different mass will flow at different rates and can localise to certain regions when drying. In the thicker regions of the sample, however, radical changes in infrared bands, such as the height ratio of amide I and II are not likely to be purely indicative of inherent structural chemistry; perturbations in intensity may also be caused by saturation effects created by the non-linear response of the detector [26]. In this scenario, one cannot simply remove distorted spectra by a quality control on thickness, as resulting 'good' spectra are likely to selectively represent certain molecules, causing a sampling bias.

The dried serum sample, whose single-point spectra are shown in Figure 3, was also measured by infrared transmission imaging to further emphasise this problem (Figure 4). A 5×5 tile mosaic was captured, representing a total sampling area of ~3.5 mm × 3.5 mm. As shown by the single-point spectra in Figure 3 (and also the total intensity of absorbance and integrated protein area in the abstract

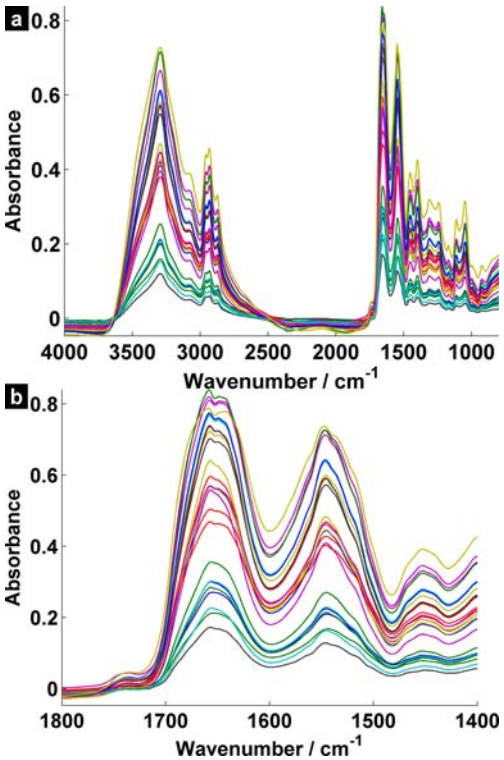

Figure 3 (**a**) Transmission single-point spectra of the >100 kDa dried serum taken from different regions across the sample with a focus on the amide band shapes in (**b**).

figure), the >100 kDa fraction sample has not dried evenly. Beyond thickness differences, due to the complex nature of the molecules contained within the serum, different spectral profiles can be classified (Figure 4a). Figure 4b reflects the first derivative mean spectrum of the classes upon which the clustering was based. As observed in the large shoulders of the amide I in certain single-point spectra (Figure 3b), the derivative features, particularly in the protein region of the spectra, suggest biochemical differences (Figure 4b).

The advantage of spatially-resolved imaging is particular apparent when addressing non-linear spectral distortions [26] as it can be seen that class 4 spectra define the affected majority with an abnormal amide I and II ratio and baseline (Figure 4c). This class of spectra spatially correspond to what appear to be cracks at the central region of the sample (Figure 4a). The loss of stray light due to scattering in the cracks, combined with the regional sample thickness, provide an unsurprising explanation for the spectral distortions and hence further illustrate the need for samples to be evenly consistent in transmission experiments. Note: The number of classes in the cluster map reflect the gross differences in the spectra illustrating the inherent non-uniformity of the dried sample which could clearly have a detrimental effect on any diagnostic model.

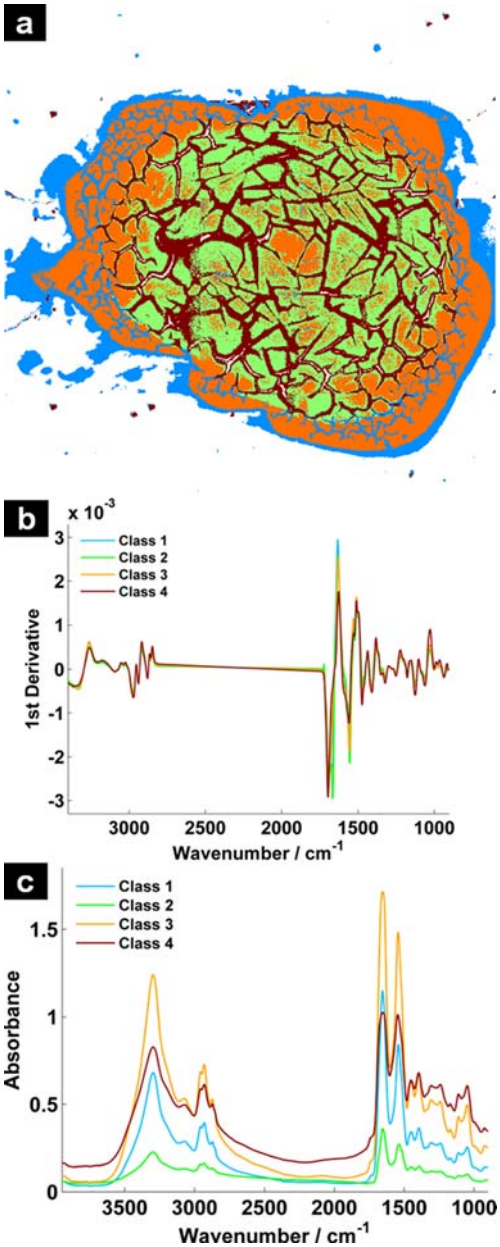

Figure 4 Image analysis of the dried >100 kDa serum sample; (**a**) 4 class cluster map; mean 1st derivative spectra (**b**) and corresponding raw mean spectra of the classes displayed in (**c**).

The same imaging process was applied to a dried sample from the 10–100 kDa fraction. A 4 × 4 tile mosaic was captured, representing a total sampling area of ~2.8 mm × 2.8 mm. Interestingly the sample appeared to be more uniform in thickness than the >100 kDa fraction, as observed by the total intensity of absorbance heat map in Figure 5a. This is possibly due to the reduced complexity of protein-related compounds in the molecular weight range and the sample was also more dilute than the >100 kDa fraction. In this case, transmission-mode infrared analysis may be more straightforward.

Once more, cluster analysis was applied to the image after quality control to remove non-sample pixel spectra. To look beyond thickness, the spectra were vector normalised and transformed to the first derivative. The pseudo-colour cluster map (Figure 5b) describes the clustering of 3 classes of spectra. It is apparent that while the molecules appear to be more evenly dispersed in the sample, the 'coffee-ring' effect still holds and molecules of different spectral profiles can be seen by the mean representative first derivative spectra (Figure 5c). Figure 5d exhibits the corresponding raw spectra of each class.

There is no apparent distortion in baseline or saturation effect in the essential fingerprint and methylene-related regions of the spectra. This result provides a good indication that transmission sampling and analysis of the dried 10–100 kDa fraction may be more practically viable than the >100 kDa fraction.

3.2 ATR measurements

Direct application of the serum sample to the ATR crystal is a popular method due to the minimal sample preparation and high reproducibility [1, 8, 27–30]. While the technique does not suffer [31, 32] the same spectral perturbations that are found in transmission-mode measurements, such as Mie and Resonant Mie related scattering [33–37], there are some drawbacks to ATR. Data interpretation can be just as complex with ATR due to the wavelength dependence of the penetration depth, causing spectral distortion [4]; the peak intensities in an ATR spectrum will increase with increasing wavelength. This is because in an ATR experiment, the depth to which the sample is penetrated by the infrared beam is a function of wavelength. Correction for this effect is standard practice but it should be noted that this is only valid if the sample is significantly thicker than the penetration depth of the longest wavelength in the spectrum.

Additionally, liquid-ATR based studies suffer from dispersion effects due to water content [38]. As a result, there have been reports of non-proportionality of the observed absorbance against actual concentration in protein samples for example. It also appears that the extent of this effect can vary from sample to sample [39, 40].

The obvious alternative is to apply the sample to the ATR crystal and wait for it to dry before analysis. The question then becomes; how to decide when the sample is ready for data acquisition? As the sample dries the concentration and therefore its relative refractive index will change. This causes further

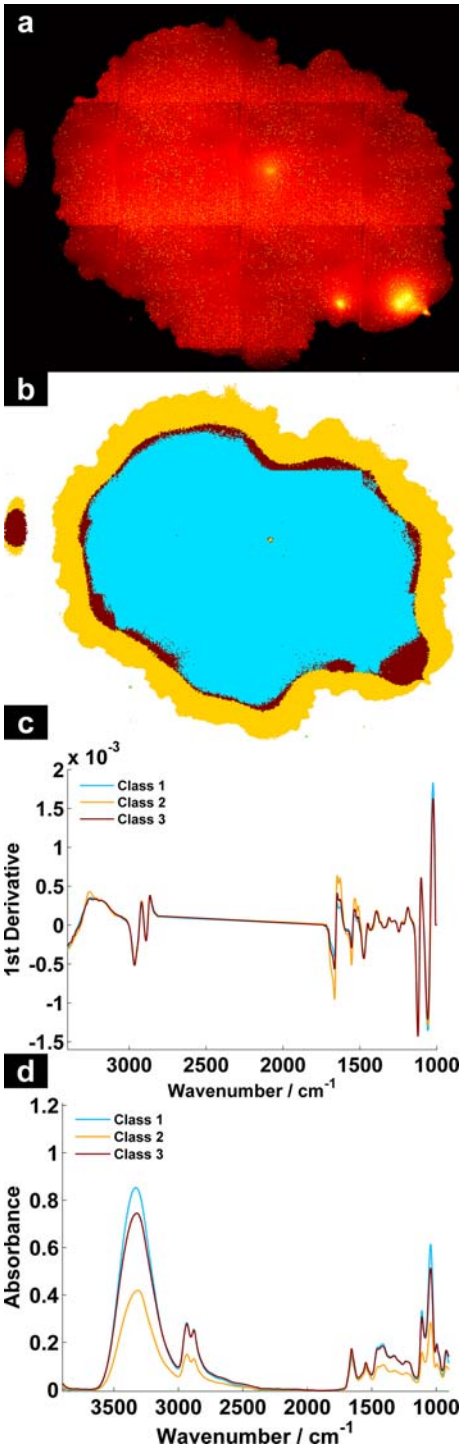

Figure 5 Imaging analysis of the 10–100 kDa dried serum sample. The total sampling area was ~2.8 mm × 2.8 mm (**a**) Total intensity of absorbance heat map; (**b**) *k*-means cluster map displaying 3c lasses; (**c**) mean 1st derivative spectra for each class and (**d**) the corresponding raw spectra.

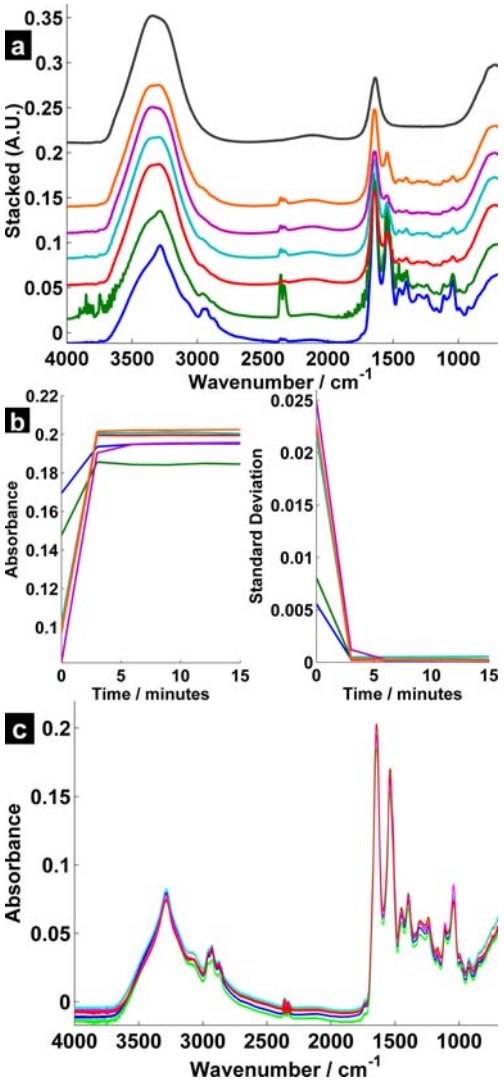

Figure 6 ATR spectra recorded for 6 different samples (each colour represents a sample); (**a**) Water (black, top) and sample spectra acquired immediately after the serum was applied to the crystal with water spectrum (**b**, left panel). The peak height intensity of the amide I band, calculated for each raw spectrum acquired every 3 minutes for one hour (total of 21 spectra). (**b**, right panel) The standard deviation of peak height intensity measured for every time point in the dataset and then re-calculated every time a spectrum was removed from T0 onwards. (**c**) Displays the 17 remaining spectra for each sample from 9–60 minutes.

spectral distortions, such as the observed differences in the baseline of the spectra [40]. To further understand this in the context of our experiment, one spectrum was acquired every three minutes over the course of an hour. A further 5 serum samples from different patients were used as distortions are known to vary from sample to sample.

Figure 6 displays the raw spectrum collected for each sample in the >100 kDa fraction. Figure 6a dis-

plays the initial spectrum recorded for the different samples respectively (in different colours) and for comparison a pure water spectrum recorded under identical conditions (top). There are experimental factors that can cause variability at this stage, namely drying rates (ambient temperature and humidity) and human error (manual application and the time taken from application to spectral acquisition). Many of the spectra display the typical dominant water absorptions over the amide I region [38, 41, 42] and the water combination band present in the baseline at ~2120 cm^{-1} [43]. Logically, meaningful analysis cannot take place until the spectral variance reaches a constant level. (Assumingly, this variance is caused by the changing concentration of the sample as it dries). To measure the impact of baseline distortions due to changing water content, the raw amide I peak intensity was measured for each time point in each sample. On first inspection the value seemed to stabilise after 3 minutes. (Note: there was a ±0.02 discrepancy in peak intensity across the samples, which may have been due to human error in sample loading or inter-sample concentration differences) (Figure 6b). To determine how many of the initial spectra should be discarded as unrepresentative, the standard deviation of the peak intensity was calculated for the total dataset (21 spectra, 0–60 minutes). Each initial time point was removed sequentially and the standard deviation of the dataset recalculated to detect when the baseline had stabilised (for example, time point 6 represents the standard deviation of the spectra acquired from 6–60 minutes). For this dataset, it appears that the spectra were reproducible from 9 minutes onwards. Here the data were all collected on the same day, however in a large-scale study, this time point could fluctuate considerably, depending on day-to-day instrumentation and environmental conditions. To allow for the acquisition of reliable and consistent data, the drying time prior to measurement may require extension. Figure 6c displays the remaining 17 spectra per sample which were acquired from 9–60 minutes. Per sample, the overlap of spectra is indicative of excellent reproducibility. In each case, however, the baseline still appears to suffer from slight distortion which may suggest that water compensation may still be required if one were to probe the entire wavelength range during analysis.

The experiment was applied to the same samples using the 10–100 kDa fraction. These fraction samples were less viscous than their heavier counterparts and displayed greater water absorbance in their immediate ATR spectra (Figure 7a). Using the same approach as before, the standard deviation of the peak height intensity of the amide I was measured. The standard deviation (as a function of decreasing inclusive time point spectra) took much longer to stabilise than the >100 kDa fraction. This

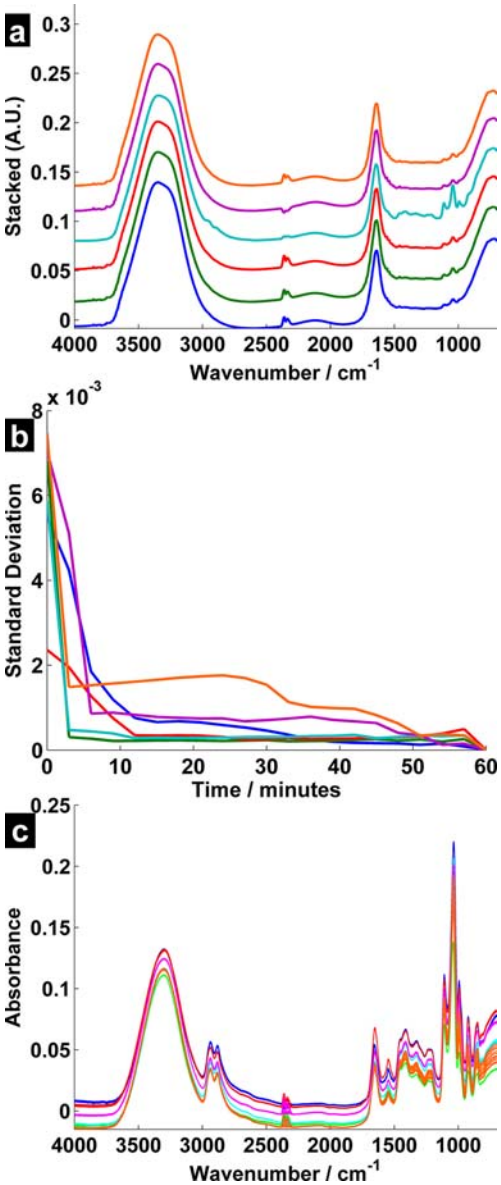

Figure 7 ATR spectra recorded for the 6 different BPH samples using the 10–100 kDa fraction. Sample spectra were acquired every 3 minutes for one hour (a total of 21 spectra each); (**a**) Sample spectra acquired immediately after the serum was applied to the crystal. (**b**) Standard deviation of amide I peak intensity measured for every time point in the dataset and then re-calculated as spectra were removed from T0 onwards; (**c**) The remaining 13 spectra for each sample from 35–60 minutes.

we attribute to the more dilute sample taking longer to dry on the ATR crystal. Most samples seemed to stabilise after 12 minutes, however, it could be argued that many took over 30 minutes (Figure 7b). Figure 7c displays the inclusive 13 spectra per sample for the range 35–60 minutes. With the exception of one sample, intra-sample group reproducibility ap-

peared to be very good, although it does highlight the issue of sample-to-sample variation.

It would appear in the case of the 10–100 kDa fraction, further experimentation would be necessary to enhance the robustness of the method, possibly by exploring the use of controlled drying mechanisms.

4. Conclusion

It has been shown that both ATR and transmission measurements have advantages and limitations. It is clear that there is still much scope for the use of either method.

It is important not to immediately search for potential spectral biomarkers when studying disease state classification projects. This should be explored only after careful consideration of the limitations of the various methods and resolution of spectral artefacts.

As remarked upon initially, the method of choice is very much dependent on the sample and the intended future use. The application of ATR to serum and plasma sample analysis is currently highly favoured in the community [7, 8, 29, 30]. In our experience we found the technique to be fairly practical, especially for the larger molecular weight fraction, producing high reproducibility. An obvious further benefit is the ability to avoid issues with sample thickness inconsistencies, as exampled by the >100 kDa fraction where distorted amide I and II peak ratios present in some transmission spectra (Figure 4c) were not observed in the equivalent ATR spectra (Figure 6c).

There is a concern, however, over water-associated distortions that remain evident in the ATR spectra of certain samples. Despite this, with little or no sample preparation, ATR allows for the delivery of rapid information. This is particularly useful for diagnostic applications when a result is required urgently. Unless a multi-ATR crystal device is created, however, it is not likely to be high-throughput in a practical sense. This is due to the time required for each sample to dry one-by-one. For instance we found that the drying time required in order to reach a stable state for spectral reproducibility could vary from ~9 to 12 or even 30 minutes, depending on sample type and control thresholds. Therefore for particularly dilute samples, controlled drying mechanisms may be required. Finally, since the ATR crystal needs to be cleaned between analyses, samples are destroyed and so can never be re-measured.

Sample preparation for transmission measurements is clearly more challenging. Recently, Ollesch et al. have successfully addressed the issue of reproducibility of dried blood-related materials by the application of a robotic spotting system, in combination with vacuum drying [6]. A preparation technique for a high volume of dried samples offers the ability of rapid screening. There is potential for the use of infrared imaging to be applied in this configuration for the evaluation and monitoring of sample quality control requirements. This is a promising technological advancement and could lead to an automated, high-throughput system to be utilised in a clinical setting, with the option of sample archiving, if desired.

Acknowledgements We would like to acknowledge the EPSRC for financial support for CH (EP/I027440/1) and the EPSRC/RSC studentship for GM. GC acknowledges studentship support from the University of Manchester.

Author biographies Please see Supporting Information online.

References

[1] H. M. Heise, R. Marbach, G. Janatsch, and J. D. Kruse-Jarres, Analytical Chemistry **61**, 2009–2015 (1989).
[2] G. Janatsch, J. D. Kruse-Jarres, R. Marbach, and H. M. Heise, Analytical Chemistry **61**, 2016–2023 (1989).
[3] J. D. Kruse-Jarres, G. Janatsch, U. Gless, R. Marbach, and H. M. Heise, Clinical Chemistry **36**, 401–402 (1990).
[4] H. Fabian, P. Lasch, and D. Naumann, Journal of Biomedical Optics **10**, 1–10 (2005).
[5] W. Petrich, K. B. Lewandrowski, J. B. Muhlestein, M. E. H. Hammond, J. L. Januzzi, E. L. Lewandrowski, R. R. Pearson, B. Dolenko, J. Fruh, M. Haass, M. M. Hirschl, W. Kohler, R. Mischler, J. Mocks, J. Ordonez-Llanos, O. Quarder, R. Somorjai, A. Staib, C. Sylven, G. Werner, and R. Zerback, Analyst **134**, 1092–1098 (2009).
[6] J. Ollesch, S. L. Drees, H. M. Heise, T. Behrens, T. Bruning, and K. Gerwert, Analyst **138**, 4092–4102 (2013).
[7] J. R. Hands, P. Abel, K. Ashton, T. Dawson, C. Davis, R. W. Lea, A. J. S. McIntosh, and M. J. Baker, Analytical and Bioanalytical Chemistry **405**, 7347–7355 (2013).
[8] K. Gajjar, J. Trevisan, G. Owens, P. J. Keating, N. J. Wood, H. F. Stringfellow, P. L. Martin-Hirsch, and F. L. Martin, Analyst **138**, 3917–3926 (2013).
[9] H. Lilja, A. T. K. Cockett, and P. A. Abrahamsson, Cancer **70**, 230–234 (1992).
[10] V. M. Velonas, H. H. Woo, C. G. dos Remedios, and S. J. Assinder, International Journal of Molecular Sciences **14**, 11034–11060 (2013).
[11] J. Hansen, M. Rink, M. Graefen, S. Shariat, and F. K. H. Chun, Molecular Diagnosis and Therapy **17**, 1–8 (2013).

[12] C. A. Evans, A. Glen, C. L. Eaton, S. Larré, J. W. F. Catto, F. C. Hamdy, P. C. Wright, and I. Rehman, Proteomics – Clinical Applications **3**, 197–212 (2009).
[13] D. K. Ornstein and D. R. Tyson, Urologic Oncology: Seminars and Original Investigations **24**, 231–236 (2006).
[14] J. J. Jayapalan, K. L. Ng, A. H. Razack, and O. H. Hashim, Electrophoresis **33**, 1855–1862 (2012).
[15] R. Harris, S. U. Patel, P. J. Sadler, and J. H. Viles, Analyst **121**, 913–922 (1996).
[16] L.-L. Cho and K.-B. Huang, Forensic Science Journal **11**, 33–40 (2012).
[17] S. Salehpour and M. A. Dubé, Macromolecular Reaction Engineering **6**, 85–92 (2012).
[18] J. Wang, M. Sowa, H. H. Mantsch, A. Bittner, and H. M. Heise, TrAC – Trends in Analytical Chemistry **15**, 286–296 (1996).
[19] P. Bassan, J. Lee, A. Sachdeva, J. Pissardini, K. M. Dorling, J. S. Fletcher, A. Henderson, and P. Gardner, Analyst **138**, 144–157 (2013).
[20] H. Brooke, D. L. Perkins, B. Setlow, P. Setlow, B. V. Bronk, and M. L. Myrick, Applied Spectroscopy **62**, 881–888 (2008).
[21] J. Filik, M. D. Frogley, J. K. Pijanka, K. Wehbe, and G. Cinque, Analyst **137**, 853–861 (2012).
[22] P. Bassan, A. Sachdeva, J. Lee, and P. Gardner, Analyst **138**, 4139–4146 (2013).
[23] T. Vahlsing, U. Damm, V. R. Kondepati, S. Leonhardt, M. D. Brendel, B. R. Wood, and H. Michael Heise, Journal of Biophotonics **3**, 567–578 (2010).
[24] C. Hughes, J. Iqbal-Wahid, M. Brown, J. H. Shanks, A. Eustace, H. Denley, P. J. Hoskin, C. West, N. W. Clarke, and P. Gardner, Journal of Biophotonics **6**, 73–87 (2013).
[25] R. D. Deegan, O. Bakajin, T. F. Dupont, G. Huber, S. R. Nagel, and T. A. Witten, Nature **389**, 827–829 (1997).
[26] J. Grdadolnik, Acta Chimica Slovenica **50**, 777–788 (2003).
[27] H. M. Heise and A. Bittner, in: Infrared Spectroscopy: New Tool in Medicine (SPIE, San Jose, CA, 1998) pp. 2–12.
[28] E. Diessel, P. Kamphaus, K. Grothe, R. Kurte, U. Damm, and H. M. Heise, Applied Spectroscopy **59**, 442–451 (2005).
[29] M. Khanmohammadi, A. B. Garmarudi, M. Ramin, and K. Ghasemi, Microchemical Journal **106**, 67–72 (2013).
[30] D. Perez-Guaita, J. Ventura-Gayete, C. Pérez-Rambla, M. Sancho-Andreu, S. Garrigues, and M. De la Guardia, Microchemical Journal **106**, 202–211 (2013).
[31] H. J. Gulley-Stahl, S. B. Bledsoe, A. P. Evan, and A. J. Sommer, Appl Spectrosc **64**, 15–22 (2010).
[32] S. G. Kazarian and K. L. Chan, Analyst **138**, 1940–1951 (2013).
[33] P. Bassan, H. J. Byrne, F. Bonnier, J. Lee, P. Dumas, and P. Gardner, Analyst **134**, 1586–1593 (2009).
[34] P. Bassan and P. Gardner, in: Biomedical Applications of Synchrotron Infrared Microspectroscopy: A Practical Approach, D. Moss (ed.) (The Royal Society of Chemistry, 2011), pp. 260–276.
[35] P. Bassan, A. Kohler, H. Martens, J. Lee, H. J. Byrne, P. Dumas, E. Gazi, M. Brown, N. Clarke, and P. Gardner, Analyst **135**, 268–277 (2010).
[36] P. Bassan, A. Sachdeva, A. Kohler, C. Hughes, A. Henderson, J. Boyle, J. H. Shanks, M. Brown, N. W. Clarke, and P. Gardner, Analyst **137**, 1370–1377 (2012).
[37] A. Köhler, J. Sulé-Suso, G. D. Sockalingum, M. Tobin, F. Bahrami, Y. Yang, J. Pijanka, P. Dumas, M. Cotte, D. G. Van Pittius, G. Parkes, and H. Martens, Applied Spectroscopy **62**, 259–266 (2008).
[38] M. Hancer, R. P. Sperline, and J. D. Miller, Applied Spectroscopy **54**, 138–143 (2000).
[39] J. J. Max and C. Chapados, Applied Spectroscopy **53**, 1045–1053 (1999).
[40] M. E. Goldberg and A. F. Chaffotte, Protein Science **14**, 2781–2792 (2005).
[41] Y. Maréchal, Journal of Molecular Structure **1004**, 146–155 (2011).
[42] H. Martens, S. W. Bruun, I. Adt, G. D. Sockalingum, and A. Kohler, Journal of Chemometrics **20**, 402–417 (2006).
[43] G. Birarda, G. Grenci, and L. Vaccari, Microscopy: Science, Technology, Applications and Education, edited by A. Mendez-Vilas and J. Diaz (Formatex Research Center, Badajoz, Spain, 2010) 422–432 (2010).

